Comparison Study on Immobilization of Ag-Doped TiO_2 using Normal and Reverse Methods for Photodegradation of Methylene Blue Dye

Nurul Izzah Roslan[1,2], Nur Izzati Nabilah Zanal[1,3], Nur Hidayatul Syazwani Suhaimi[1], Rahil Azhar[1], Nur Syamimi Adzis[1], Mohamad Afiq Rosli[1] and Wan Izhan Nawawi Wan Ismail[1]*

[1]Faculty of Applied Sciences, Universiti Teknologi MARA, 02600 Arau, Perlis, Malaysia

[2]Chemical Laboratory, FELCRA Plantation Services Sdn. Bhd., Bandar Baru Seberang Perak, 36800 Kg Gajah, Perak

[3]Multisafe Sdn Bhd, Lot 764, Bidor Industrial Estate, 35500, Bidor, Perak Darul Ridzuan, Malaysia

*Corresponding author (e-mail: wi_nawawi@uitm.edu.my)

Immobilized Ag/TiO_2 was prepared using reverse (R) and normal (N) methods, employing epoxidized natural rubber (ENR-50) and polyvinyl chloride (PVC) as polymer binders to form a Ag-TiO_2/ENR/PVC (ATEP(R)) plate in order to address the solvent interference issue. The immobilization of TiO_2 was performed prior to the photodeposition of Ag (50, 100 and 400 ppm), by irradiation with a 250-Watt metal halide lamp for 90 minutes. TiO_2 was coated onto glass plates using a dip-coating technique. Methylene blue (MB) was employed as a model pollutant to evaluate the photocatalytic activity of the prepared immobilized Ag/TiO_2. Several instruments were used for characterization, including Ultraviolet-Visible Diffuse Reflectance Spectroscopy (UV-Vis DRS), Fourier Transform Infrared spectroscopy (FTIR) and photoelectrochemical (PEC) analysis. The UV-Vis DRS results indicated that the band gap for 100 ppm of Ag-TiO_2/ENR/PVC (100-ATEP(R)) was 2.42 eV, with its absorption edge shifted towards the visible region. FTIR analysis showed a peak at 1382 cm^{-1}, confirming the successful doping of Ag onto TiO_2, while a less intense peak for OH at 3400 cm^{-1} indicated the low hydrophilicity of the photocatalyst. PEC analysis revealed that 100-ATEP(R) exhibited higher current density in linear sweep voltammetry (LSV) curves, lower charge transfer resistance in Nyquist plots and higher photocurrent response in chronoamperometry (CA) plots, compared to TiO_2/ENR/PVC (reverse) TEP(R). All immobilized ATEP(R) samples showed excellent photocatalytic degradation of methylene blue (MB) dye and achieved 52 % decolorization within 1 hour of light irradiation, indicating higher photocatalytic activity compared to the normal method. The photocatalytic degradation of all samples followed the pseudo-first-order reaction model of Langmuir Hinshelwood, with R^2 values above 0.90. The results indicate that this new immobilization method may be used for all photocatalysts as it can prevent disruption of the immobilized photocatalyst by the solvent, which is a disadvantage of the normal immobilization method.

Keywords: Immobilized TiO_2; reverse method; photocatalytic degradation; ENR/PVC immobilization

Received: August 2024; Accepted: October 2024

Water is essential to all living organisms on Earth and plays an important role in the hydrological cycle. Water pollution has become a significant environmental issue due to industrial activities. Industrial effluents, containing organic and inorganic contaminants such as pesticides, fertilizers and residual dyes, are regularly discharged into water bodies without proper treatment [1]. Textile dyes have become one of the major contributors to environmental degradation and water pollution as they contain very high concentrations of harmful recalcitrant colorant pollutants and toxic compounds that can persist in the environment for long periods [2, 3].

According to Oladoye et al. (2022), methylene blue (MB) is a synthetic dye commonly used in the textile industry [4]. Synthetic dyes are difficult to biodegrade and persist in the environment. Therefore, several approaches have been developed to treat wastewater, including adsorption, physical, biological, and chemical treatments [5]. Advanced oxidation processes (AOP) are a class of chemical treatment alternatives that can effectively degrade these synthetic dyes. AOPs, such as photocatalytic degradation, are environmentally friendly techniques that degrade organic pollutants into less hazardous or non-toxic components [6].

Currently, titanium dioxide (TiO_2) is widely utilized in photocatalysis for dye degradation due to its unique properties, including availability, low cost, high chemical stability, non-toxicity and good photostability [7]. However, pure TiO_2 has low solar and quantum efficiency in practical applications

due to its broad bandgap (3.2 eV) and increased recombination of charge carriers [8]. Thus, modifying TiO_2 is necessary to enhance its photocatalytic performance in dye degradation. Several experiments have been conducted to enhance the photocatalytic efficiency of TiO_2 by doping it with noble metals such as silver (Ag), platinum (Pt) and palladium (Pd), or nonmetals such as carbon (C), nitrogen (N), and phosphorus (P) [9].

Immobilization of TiO_2 is the process of attaching TiO_2 onto a solid support, which can improve its stability, photocatalytic activity and biocompatibility [10]. On the other hand, doping techniques allow the modification of a semiconductor's activity by utilizing the properties of the dopant in combination with several metals to reduce the semiconductor's band gap [11]. Ag is an example of a noble metal that helps in lowering the conduction band of TiO_2, reducing the band gap energy and enabling TiO_2 to absorb light in the visible region [12]. According to Sun et al. (2024), Ag is a stable, cost-effective, non-hazardous metal with excellent thermal and electrical conductivity [13].

Previously, immobilized Ag/TiO_2 was commonly prepared using the normal method, where Ag photodeposition was done prior to immobilization. It exhibited lower photocatalytic activity towards dye degradation due to the solvent interference that occurs during photodeposition. The solvent used can interact with both Ag and TiO_2 and disrupt charge transfer at the Ag/TiO_2 interface, hence influencing performance [14]. Thus, this study aims to prepare immobilized Ag/TiO_2 photocatalysts using a reverse method, where immobilization of TiO_2 is done prior to Ag photodeposition. The photocatalytic performance of both normal and reverse methods was evaluated by photodegradation of MB dye, the target pollutant.

EXPERIMENTAL

Chemicals and Materials

TiO_2 powder (Degussa P25; 20 % rutile, 80 % anatase) was supplied by Merck. Epoxidized natural rubber (ENR-50) and polyvinyl chloride (PVC), utilized as Polymer binders to hold TiO_2 nanoparticles, were supplied by Kumpulan Guthrie Sdn. Bhd and Petrochemicals (M) Sdn. Bhd, respectively. Distilled and deionized water was utilized as the solvent for all experiments, and methylene blue (MB) dye powder with 96–100 % dye content, supplied by Sigma-Aldrich, United States, was used as a model pollutant. Silver nitrate ($AgNO_3$), used as a Ag precursor, was supplied by System Chemicals, Malaysia.

A glass plate measuring 10 x 1.5 x 0.2 cm (L x H x B) was utilized as a support material for TiO_2 immobilization. A 55-Watt fluorescent lamp model Firefly/E27 was used as the light source for the photodegradation process. The TiO_2 formulation was stored in a 250 mL Schott bottle and the mixture was kept homogenized using a Grant-bio multipurpose orbital shaker. The 1000 mg L^{-1} stock solution of MB was prepared by dissolving 1.0 g of MB powder with pure water in a 1 L volumetric flask. For the photocatalytic study of MB dye, the MB stock solution was diluted to 12 mg L^{-1} using distilled water.

Immobilization of Titanium Dioxide (TiO_2) with ENR/PVC

The ENR-50 solution was prepared by refluxing 24. 8 ± 0. 5 g of ENR-50 in 250 mL toluene at 88-90 °C until the compound was fully dissolved, resulting in an adhesive-like, sticky solution. A specific quantity of PVC powder was dissolved in 35 mL dichloromethane (DCM) via sonication for 1 h to prepare the PVC solution. For the preparation of the dip-coating solution containing P-25 TiO_2 nanoparticles, the appropriate quantities of ENR-50 solution and PVC powder were added to 6 g of a mixture of toluene and dichloromethane. For the formulation of the dip-coating solution, various amounts of PVC powder (0.40, 0.60, 0.80, 1.00, and 1.20 g) were mixed with the respective amounts of ENR-50 in 35 mL of the solvent mixture. The mixture was sonicated using an ultrasonic machine until homogenization was achieved, typically after 9 hours, when no more P-25 TiO_2 particles were observed at the bottom of the bottle. A similar series of samples, where the total weight remained constant, but the amount of ENR-50 varied, was prepared to establish the optimum amount of ENR-50.

The P-25 TiO_2/ENR/PVC composite was coated on a clean glass plate (47 mm × 70 mm, 2 mm thickness) using the dip-coating technique. Each glass plate was dried in an oven at 100 °C for at least 30 min and then weighed carefully using an analytical balance (Denver Instrument Company, model AA-160). At the same time, the prepared homogenized solution was poured into a glass coating cell. Then, each glass plate was dipped to a depth of 5.6 cm (26.3 cm^2) and left for 5 seconds in the dip-coating solution. It was subsequently pulled up manually at a consistent pulling rate between each dipping to obtain a uniform deposition of the photocatalyst.

The coated glass plate was dried completely using an air blower to vaporize the solvent. Next, the smooth side of the coated glass plate was scraped off and again carefully weighed. The difference in weight between the blank glass plate and its corresponding coated plate represented the weight of the immobilized P-25 catalyst. The coating, drying, and weighing procedures were repeated until 40 mg or the equivalent catalyst loading of 1.5 mg cm^{-2} was achieved.

Immobilized Ag-doped TiO_2 by the Normal Method

The Ag/TiO_2 solution was prepared by mixing 13 g of the Ag/TiO_2 catalyst with 100 mL of distilled water in a 250-mL reagent bottle. The solution was shaken for 30 minutes using a Grant-bio orbital shaker (model PSU-20i) to homogenize the Ag/TiO_2 solution before coating. The immobilized Ag/TiO2 was prepared using the brush coating method, where Ag-doped TiO_2 solution was coated on top of the thin layer of ENR/PVC with a dimension of 5 x 6 cm attached to the 13 x 5 cm (L x H) glass plate. The sample was labelled as ATEP, and the catalyst loading of the immobilized Ag-doped TiO2/ENR/PVC was fixed at 0.1 ± 0.05 g, as weighed by an electronic weighing balance. The immobilized $Ag\text{-}TiO_2$/ENR/ PVC was dried using a hot air blower, Khind HD14000.

Immobilized Ag-doped TiO_2 by the Reverse Method

Immobilized Ag/TiO2 was synthesized using a reverse method. Solutions containing 50, 100, and 400 ppm of Ag to be doped onto the immobilized TiO_2 were prepared using silver nitrate ($AgNO_3$) as the Ag precursor. The reverse photodeposition method was conducted by pouring about 80 mL of a solution of aqueous $AgNO_3$ in 50 % IPA into a Schlenk tube. The glass plate coated with immobilized TiO2 was hung by a thread and immersed in the solution. The Schlenk tube was placed under nitrogen purging for 30 minutes to ensure suitable levels of oxygen and moisture during preparation. Then, the immobilized TiO2 and $AgNO_3$ aqueous solution were irradiated with a 250-Watt metal halide lamp for about 1.5 h to form immobilized Ag/TiO2.

Photocatalytic Degradation Study with Methylene Blue Dye

For the photocatalytic degradation study, 12 mg L^{-1} of MB dye was used as the model organic pollutant. 15 mL of the MB dye solution was measured into a 15 x 10 x 8 cm (L x B x H) glass cell. The prepared immobilized Ag/TiO_2 was then immersed in the solution. The solution was irradiated with a 55-Watt fluorescent lamp for 60 min with intervals every 15 minutes. An aerator source, aquarium pump model NS 7200, was used to supply oxygen for the reaction at 15 mL/min. A HACH DR 1900 spectrometer was used to determine the percentage of decolorization of MB from the photodegradation process at a wavelength of 661 nm. The k-value and linear correlation value were calculated by plotting these values against irradiation or contact time. The findings were transformed into ln C_o/C, where C_o is the absorbance of the starting concentration, and C is the absorbance at any time (t). The slope of the line was used as the pseudo-first-order rate constant in the Langmuir-Hinshelwood rate model as Equation 1.

$$\text{Degradation rate (\%)} = \frac{C}{\text{Co}} \quad \text{x 100 \%} \qquad (1)$$

Where C_O is the initial concentration and C is the final concentration.

Characterization Methods

Fourier Transform Infrared - Attenuated Total Reflectance (FTIR-ATR) spectroscopy (Perkin-Elmer, model system 2000 FTIR) was used to detect the functional groups or bonds in TiO_2 and Ag/TiO_2 in the range 600-4000 cm^{-1}. X-ray Diffraction (XRD) was employed to analyse the crystalline phases, sizes, structures and micro-strains of the TiO_2 and Ag/TiO_2 nanoparticles at different doping percentages using an X-ray diffractometer (RIGAKU/XRD D/MAX 2200V/PC) with Cu Kα radiation at a wavelength of 1.5418 Å at 50 kV and a Lynx Eye detector. FESEM equipped with Energy Dispersive X-Ray analysis (EDX) was utilized using a Hitachi SU8020 instrument to determine the surface morphologies of TiO_2 and Ag/TiO_2, and metal dispersion on the catalyst surface. UV-Vis Diffuse Reflectance Spectroscopy (DRS, Perkin Elmer Lambda 35, USA) in the range of 200-800 nm was used to determine the light absorption edge and band gap energy of Ag/TiO_2. Photoelectrochemical (PEC) analysis was carried out to obtain linear sweep voltammetry (LSV), electrochemical impedance spectroscopy (EIS) and chronoamperometry (CA) plots which were analysed using a potentiostat by CORRTEST instrument (Model CS310M) with a three-electrode system. The system used an electro-chemical cell with Ag/AgCl as a reference electrode in 3 M NaCl and platinum as a wire counter electrode. The working electrode was ITO glass (area: 2.5 cm X 2.5 cm) and the electrolyte used was a 0.2 M Na_2SO_4 solution. The photocurrent was measured over time and 100 cm mw cm^{-2} of the light source was also supplied by Cerusal Model: TM-71 during the analysis.

RESULTS AND DISCUSSION

Characterization

Fourier Transform Infrared (FTIR) Spectroscopy

Figure 1 illustrates the FTIR spectra of the TEP and ATEP photocatalysts, measured in the range of 4000-600 cm^{-1}. FTIR analyses were carried out to determine the functional groups and surface chemistry of the photocatalysts. The spectra of all the samples showed broad absorption peaks between 3000-3400 cm^{-1}, corresponding to the stretching vibrations of hydroxyl groups (-OH) in H_2O. This indicates the presence of adsorbed H_2O molecules on the catalyst surface [15]. The absorption peak at 1600-1700 cm^{-1} indicates the bending vibrations of surface hydroxyl groups (OH) cm^{-1} [16]. The number of OH groups present in Ag-doped TiO_2 affects its photocatalytic activity as the increase in -OH functional groups may lead to a

greater number of hydroxy biradicals required in the photocatalytic degradation process and enhance the overall photocatalytic performance. Based on Figure 1, the peak representing OH in Ag/TiO_2 (50, 100, 400-ATEP) had a lower intensity compared to that in TEP,

indicating less hydrophilic behaviour. It contradicts the ideal property of a photocatalyst, which needs to possess greater hydrophilic properties for better pollutant adsorption and photodegradation. Additionally, the broad peaks observed in these regions of the modified Ag/TiO_2 sample indicate significant changes in the surface properties of TiO_2 due to Ag doping. The anatase phase of TiO_2 was confirmed through the appearance of peaks in the 650-1400 cm^{-1} region which reflect the lattice vibrations of Ti-O-Ti stretching [17]. The introduction of Ag nanoparticles into the TiO_2 lattice caused a shift in the Ti-O-Ti peaks (1400-1370 cm^{-1}) of Ag/TiO_2, as can be seen in Figure 1(b). This modification also caused XRD peak shifts, as reported by Kader et al. (2022) [18]. Therefore, the shift in the Ag/TiO_2 peak at 1382 cm^{-1} indicates the successful deposition of Ag nanoparticles on TiO_2 [9].

X-Ray Diffraction (XRD) and FESEM-EDX Mapping Analysis

The X-ray diffraction (XRD) spectra for TEP(R) and 100-ATEP(R) are shown in Figure 2. The XRD patterns were measured at 2θ = 10-80°. The XRD patterns of TEP(R) and 100-ATE(R) samples showed peaks at 101, 110, 004, 200, 105, 211, 204, 116, and 220, corresponding to TiO_2, based on JCPDS file No: 894921.

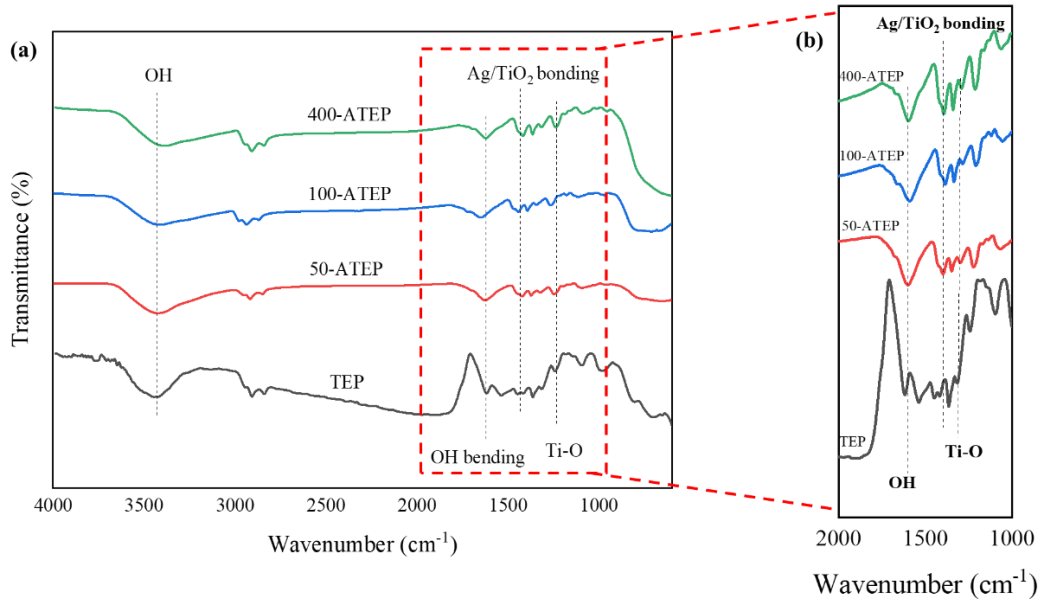

Figure 1. (a) FTIR spectra of TEP (R) and all ATEP (R) samples, and (b) Focus area enlargement of significant peaks.

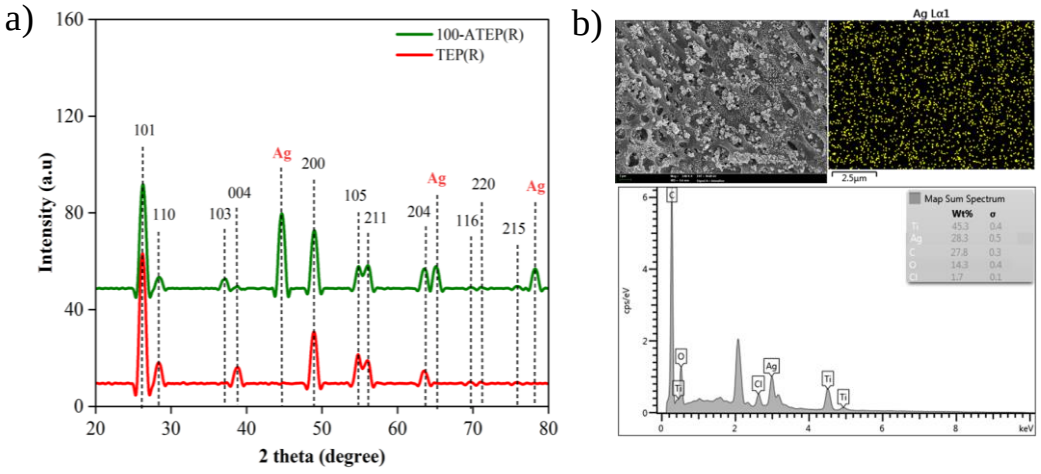

Figure 2. (a) XRD spectra of TEP(R) and 100-ATEP(R), and (b) FESEM-EDX results for 100-ATEP(R).

The additional peaks that appeared for the 100-ATEP(R) sample observed at 45, 65 and 78° were identified as peaks of elemental Ag, as previously reported by Chakhtouna et al. (2021) [19]. To further confirm the presence of Ag, 100-ATEP(R) was analysed by FSEM-EDX mapping, as shown in Figure 2 (b). Based on the mapping analysis, Ag was well distributed in the 100-ATEP(R) sample, with a composition of 28.3 % and a porous, sponge-like morphology.

UV-VIS Diffuse Reflectance Spectroscopy (UV-Vis DRS)

The band gap energies for unmodified TiO_2 (TEP) and modified 100-ATEP (100 ppm Ag-TiO_2/ENR/PVC) prepared via the normal method (N) as well as the reverse method (R) were determined by UV-Vis DRS absorption spectra, as shown in Figure 3. Based on Figure 3(a), TEP exhibited optimal performance under UV irradiation with a wavelength lower than 380 nm, but this performance gradually dropped as the wavelength increased. In contrast, 100-ATEP(N) and 100-ATEP(R) exhibited a broad absorbance peak at 400 nm that shifted towards the visible region compared to the TEP sample. However, the shift indicated that 100-ATEP(R) absorbed longer wavelengths of light (lower energy photons) compared to the 100-ATEP(N), demonstrating that the photocatalyst modified by the reverse method was responsive to visible light due to the lowering of the TiO_2 band gap energy and the SPR effect exhibited by the Ag nanoparticles [20]. On the other hand, the broader peak of 100-ATEP(R) enhanced the SPR effect due to better dispersion and smaller Ag distribution. The findings indicate that the interaction among Ag NPs led to a shift of the resonance absorption peak towards the visible region, resulting in a lower band gap energy [21]. The band gap energy (E_g) of the samples were calculated based on the Tauc plots shown in Figure 3(b) using the Tauc equation below.

$$(\alpha h\nu)^{\wedge}n = A\,(h\nu - E_g) \quad (2)$$

where A is a constant, α is the absorption coefficient, h is Planck's constant, ν is the frequency of the incident light, and E_g is the band gap energy. n can be defined as 2 or $^1/_2$, where 2 is used for a direct band gap while $^1/_2$ is used for an indirect band gap.

The band gap energies of TEP, 100-ATEP (N) and 100-ATEP(R) were calculated to be 3.13 eV, 2.47 eV, and 2.30 eV respectively. The reduced band gap energy of modified TiO_2 allowed for better absorption of light in the visible region, which is beneficial for photocatalytic applications. The reduction in the band gap energy of 100-ATEP(R) from 3.47 eV to 2.30 eV led to a shift in the absorption edge towards a longer wavelength, improving its visible light absorption and making it more effective for photocatalysis and other applications that require visible light activation.

Photoelectrochemical (PEC) Analysis

Linear Sweep Voltammetry (LSV)

Linear Sweep Voltammetry (LSV) was employed to obtain the redox properties of the photocatalyst samples. Figure 4(a) shows the LSV curves for the TEP and 100-ATEP(R) samples respectively under dark (reductive sweep) and light illumination (oxidative sweep) conditions. The results indicate that photocurrent values increased linearly with the potential values in the low potential zone before remaining constant throughout the measured time interval. The TEP sample showed lower photoresponse values under light conditions, while 100-ATEP(R) had a better photoresponse curve, thus the current density was higher under light conditions indicating that the light intensity may have minimal impact on current density [22].

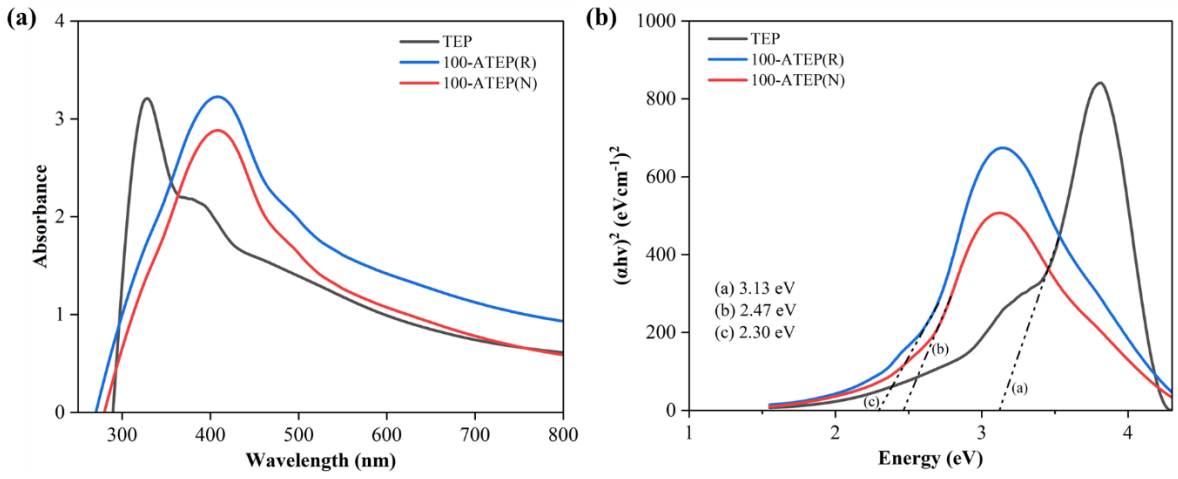

Figure 3 (a) Absorption spectra, and (b) Tauc plots for TEP, 100-ATEP(N) and 100-ATEP (R).

Furthermore, the localized surface plasmon resonance (LSPR) phenomenon in Ag nanoparticles may contribute to the increase in current density [19]. The curve was slightly higher in light compared to dark conditions at constant state potential, indicating the Ag/TiO_2 composites exhibited photoactivity in visible light due to the LSPR phenomenon which improves light absorption.

Electrochemical Impedance Spectroscopy (EIS)

Electrochemical impedance spectroscopy (EIS) analysis was performed to study the charge transfer at the photoanode-electrolyte interface [23]. Figure 4(b) shows the fitted Nyquist plots for TEP and 100-ATEP(R), respectively, which were obtained under different conditions: dark and light. A Nyquist plot represents the real impedance (Z') in the x-axis and the imaginary impedance (Z") in the y-axis. The smaller semicircle shows lower charge transfer resistance, higher conductivity and vice versa [24]. Both samples indicated that the smaller semicircle represented impedance in the presence of light, demonstrating that light improved charge transfer, reduced resistance and increased conductivity. This response is specific for photocatalytic materials in which light stimulates electrons, lowers resistance and improves electrochemical performance. The Ag-doped sample 100-ATEP showed a lower charge transfer resistance compared to the TEP sample, indicating that Ag nanoparticles had high conductivity due to the large number of free electrons available for conducting electricity. Ag conducts electricity well even in dark conditions; however, light exposure considerably boosts its conductivity. In the presence of light, Ag atoms absorb photons, which excite electrons to higher energies [25]. These energized electrons flow more freely, increasing electrical conductivity.

Chronoamperometry (CA)

Photocatalytic degradation of organic pollutants requires effective isolation and transfer of photogenerated carriers. Photocurrent response has become one of the most plausible proofs of charge separation [23]. Figure 4(c) indicates the transient photocurrent response curves for the TEP and 100-ATEP(R) samples that each consist of a light/dark cycle of 60 seconds and a 30-second gap. The TEP sample showed a lower photocurrent response compared to 100-ATEP(R). TiO_2 is a semiconductor with outstanding photocatalytic capabilities. Under UV light, TiO_2 produces electron-hole pairs (e^-/h^+); however, its broad bandgap restricts activation to UV light (5 % of the solar spectrum).

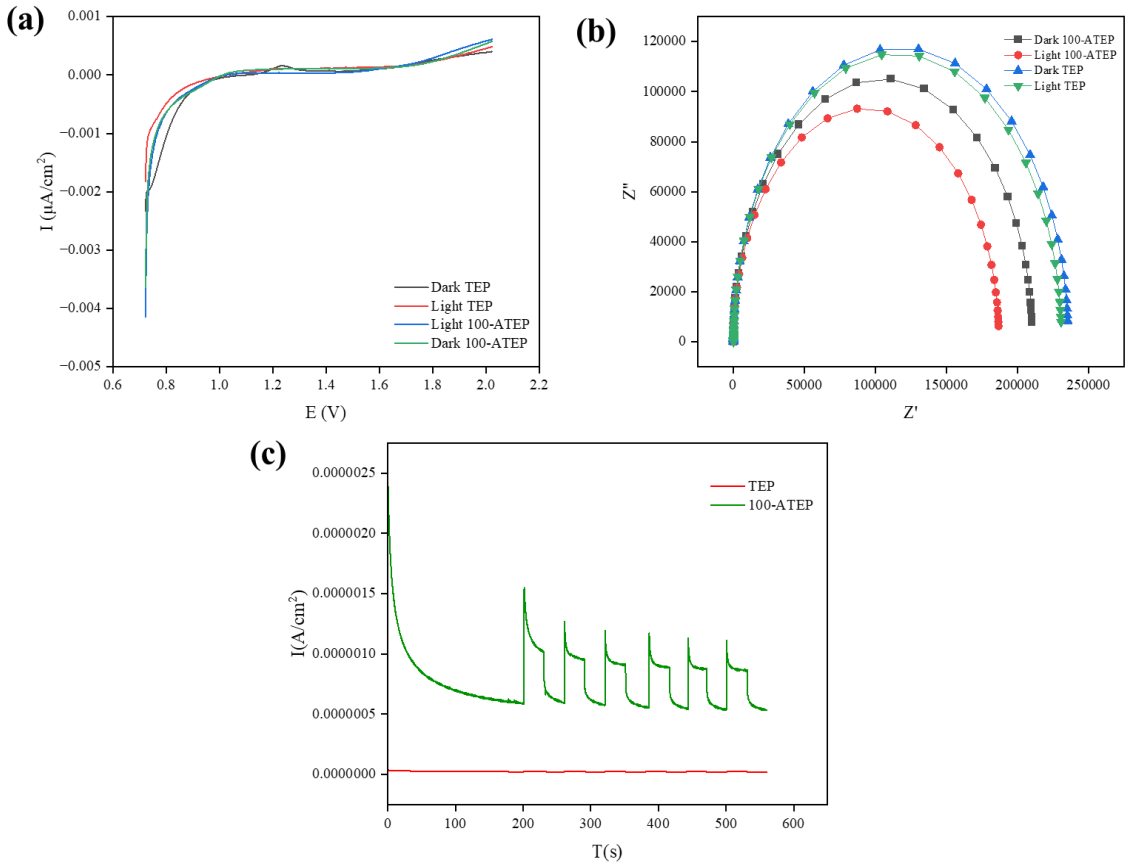

Figure 4 (a) LSV curves under dark and light conditions, (b) Nyquist plots and (c) CA plots for TEP (R) and 100-ATEP (R).

Berdakin et al. (2022) states that rapid e^-/h^+ recombination lowers overall photocatalytic efficiency and multiple cycles may compromise stability [26]. On the other hand, the 100-ATEP(R) sample showed that the Ag nanoparticles became activated TiO_2 under visible light and created a Schottky barrier that prevented recombination. Furthermore, Ag nanoparticles create energy levels near the conduction band, which promotes electron excitation [27]. Reduced recombination results in more efficient charge transfer. Thus Ag/TiO_2 maintains charge separation during multiple cycles.

Photocatalytic Degradation and Optimization Study

Photodegradation of Methylene Blue Dye

Two different preparation methods were analysed in the photocatalytic degradation study: the normal method and the reverse method. Figure 5 (a) and (c) illustrate the percentage of photocatalytic activity remaining over 60 minutes of light irradiation for the normal and reverse methods, respectively. Initially, all samples exhibited 100 % photocatalytic activity. TEP samples prepared by the normal method showed photocatalytic degradation of MB dye with 52 % decolorization after 1 hour, while 70 % decolorization was achieved by TEP prepared by the reverse method. This suggests an enhancement in the photocatalytic activity of reverse method TEP samples. However, 400-ATEP(R) showed the least decolorization of MB dye due to the increased concentration of Ag. This proves that immobilized Ag/TiO_2 prepared using the reverse method improved Ag usage, which may avoid the excess solvent problem while improving photocatalytic performance. The photocatalytic degradation rate for all samples as shown in Figure 5(b) and (d) followed the pseudo-first-order reaction of Langmuir Hinshelwood, with R^2 values exceeding 0.90.

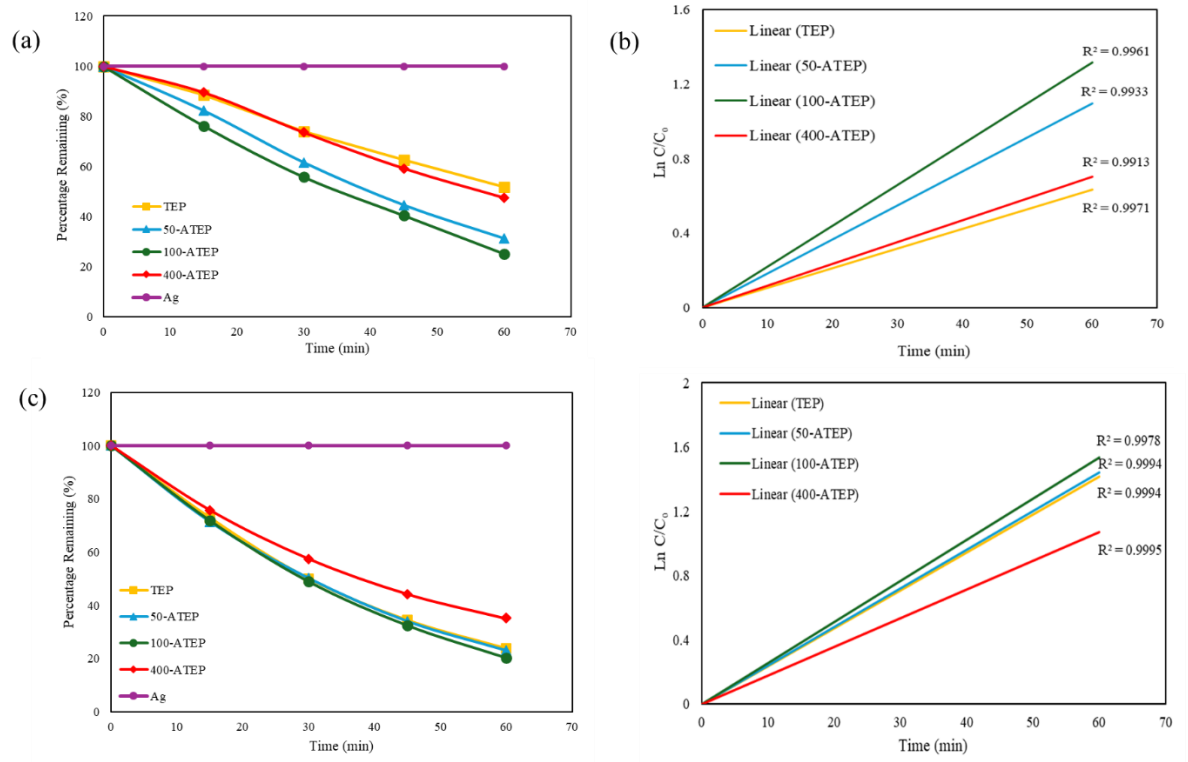

Figure 5. (a) Percentage of MB dye remaining after photodegradation of ATEP(N), (b) Linear correlations for ATEP(N), (c) Percentage of MB dye remaining after photodegradation of ATEP(R), and (d) Linear correlations for ATEP(R).

Table 1. K-values for photodegradation of MB dye.

Concentration of Ag (ppm)	Pseudo-first-order rate constant (min^{-1})	
	Normal method	Reverse method
0	0.0106	0.023
50	0.0183	0.024
100	0.0207	0.0256
400	0.0103	0.017

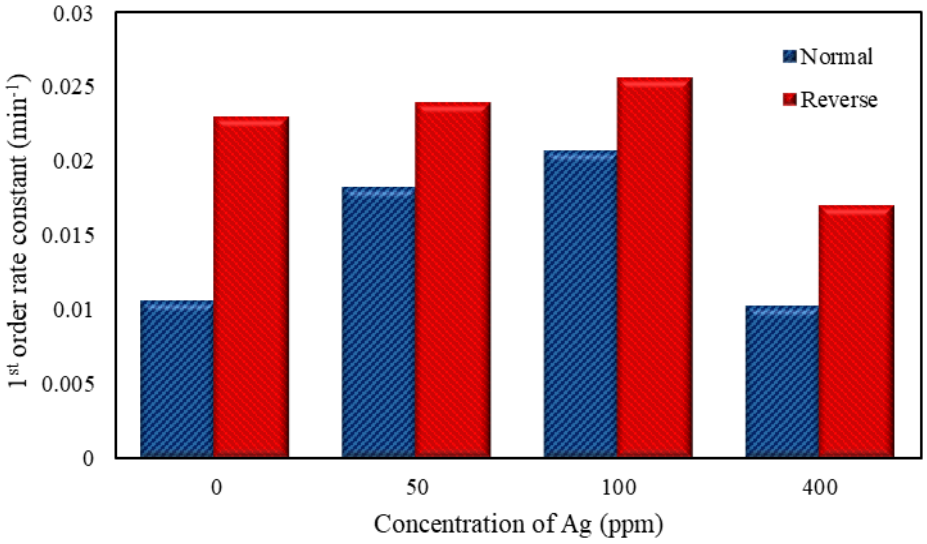

Figure 6. Comparison of K-values between normal and reverse methods.

Table 1 shows the rate constants (K-values) for all samples by two preparation methods, normal and reverse, while Figure 6 illustrates the bar graph of trends in k-values as the concentration of Ag increased. The photocatalytic degradation rates indicate that the reverse method improved the dispersion and availability of Ag nanoparticles on the TiO_2 surface. The normal method demonstrated a lower photocatalytic activity as its K-values were generally lower than for the reverse method samples, indicating a lower photocatalytic degradation of MB. This shows that Ag/TiO_2 significantly improved its photocatalytic activity with an optimum concentration of 100 ppm. Therefore, immobilized Ag/TiO_2 prepared by the reverse method improved its photocatalytic activity compared to the normal method, as it solved the solvent interaction problem.

CONCLUSION

An immobilized Ag/TiO_2 photocatalyst was successfully prepared using the reverse method. In comparison to the normal method, immobilized Ag/TiO_2 using the reverse method showed increased photocatalytic activity in terms of photodegradation of MB dye. The characterization of Ag/TiO_2 was performed using UV-Vis DRS, which indicated that the presence of deposited Ag decreased the band gap of TiO_2. The optical properties of Ag/TiO_2 were determined by PEC analysis while FTIR was used to determine the organic compounds present in the unmodified TiO_2 and modified Ag/TiO_2 samples. Ag nanoparticles were successfully doped onto the surface of TiO_2 as proved by the characterization study. The photodegradation rate of Ag/TiO_2 improved as the amount of Ag loading increased from 50 ppm to 100 ppm, before declining at 400 ppm. As a result, 100 ppm was found to be the optimum doping amount. Physical and chemical changes in the Ag/TiO_2 photocatalyst were also successfully identified by UV-Vis DRS, PEC analysis and FTIR studies.

ACKNOWLEDGEMENTS

We would like to acknowledge Universiti Teknologi MARA (UiTM) for providing all the facilities. This work was also supported by the Ministry of Higher Education (MOHE) under the Fundamental Research Grant Scheme: FRGS/1/2022/STG04/ UITM/02/1.

REFERENCES

1. Ounas, O., Foulani, A. A. El, Lekhlif, B. & Jamaleddine, J. (2020) Immobilization of TiO_2 into a poly methyl methacrylate (PMMA) as hybrid film for photocatalytic degradation of methylene blue. *Materials Today: Proceedings*, **22**, 35–40.

2. Olisah, C., Adams, J. B. & Rubidge, G. (2021) The state of persistent organic pollutants in South African estuaries: A review of environmental exposure and sources. *Ecotoxicology and Environmental Safety*, **219,** 112316.

3. Kishor, R., Purchase, D., Saratale, G. D., Ferreira, L. F. R., Bilal, M., Iqbal, H. M. N. & Bharagava, R. N. (2021) Environment friendly degradation and detoxification of Congo red dye and textile industry wastewater by a newly isolated Bacillus cohnni (RKS9). *Environmental Technology and Innovation*, **22,** 101425.

4. Oladoye, P. O., Ajiboye, T. O., Omotola, E. O. & Oyewola, O. J. (2022) Methylene blue dye: Toxicity and potential elimination technology

from wastewater. *Results in Engineering*, **16**, 100678.

5. Mishra, S. & Sundaram, B. (2023) A review of the photocatalysis process used for wastewater treatment. *Materials Today: Proceedings*.

6. Dihom, H. R., Al-Shaibani, M. M., Mohamed, R. M. S. R., Al-Gheethi, A., Sharma, A. & Khamidun, M. H. (2022) Photocatalytic degradation of disperse azo dyes in textile wastewater using green zinc oxide nanoparticles synthesized in plant extract: A critical review. *Journal of Water Process Engineering*, **47**, 102705.

7. Natar, N. S., Ghani, N. I. A., Hamzah, S. R., Rosli, M. A., Muhamad, N. A., Azami, M. S., Ishak, M. A. M., Razak, S. & Nawawi, W. I. (2022) The Role of Nitrogen-Doped TiO2 Supported by Platinum Catalyst Synthesized via Various Mode Preparations for Photocatalytic Enhancement. *Nanomaterials*, **12(22)**, 3998.

8. Li, L., Chen, X., Quan, X., Qiu, F. & Zhang, X. (2023) Synthesis of CuO_x/TiO_2 Photocatalysts with Enhanced Photocatalytic Performance. *ACS Omega*, **8(2)**, 2723–2732.

9. Adzis, N. S., Suhaimi, N. H. S., Abdul Ghani, N. I., Abd Yami, N. F. N., Muhamad, N. A., Mohd Azami, M. S. & Wan Ismail, W. I. N. (2023) Modification of Silver Oxide/Silver Doped Titanium Dioxide (Ag_2O/Ag- TiO_2) Photocatalyst Using an Immobilized Reverse Photodeposition Method for Photodegradation of Reactive Red 4 Dye. *Malaysian Journal of Chemistry*, **25(4)**, 184–198.

10. Indriani, Y., Sutanti, A. S. A. P., Ayuningtyas, M. & Widiyandari, H. (2021) A Brief Review: Immobilization of TiO_2 Photocatalyst Materials on Supporting Surfaces for Degradation of Organic Pollutants. *Materials Science Forum*, **1044**, 153–161.

11. Soundarya, T. L., Harini, R., Manjunath, K., Udayabhanu, Nirmala, B. &Nagaraju, G. (2023) Pt-doped TiO_2 nanotubes as photocatalysts and electrocatalysts for enhanced photocatalytic H_2 generation, electrochemical sensing, and supercapacitor applications. *International Journal of Hydrogen Energy*, **48(82)**, 31855–31874.

12. Gusmão, C. D. A., Palharim, P. H., Ramos, B., Gouvea, D., Rodrigues Jr, O. & Teixeira, A. C. S. C. (2024) Enhanced visible light photocatalytic VOC oxidation via Ag-loaded TiO2/SiO2 materials. *Journal of Materials Science*, **59(4)**, 1215–1234.

13. Sun, W., Gou, G., Qiu, X., Feng, Q., Zhang, K., Qin, S. & Gao, W. (2024) Research on regulation mechanism of TiO_2 photocathodic protection based on cohesive energy, defect patterns, and nanofilm size. *Journal of Materials Engineering and Performance*, **7(2)**, 1–12.

14. Khalaf, G. R., Abbas, K. N. & Abbas, A. M. (2024) Effect of solvent polarity on the physical properties and antibacterial and antifungal activity of TiO_2 and Ag/TiO_2 nanoparticles. *Brazilian Journal of Physics*, **54(3)**.

15. Kanakaraju, D., Kutiang, F. D. A., Lim, Y. C. & Goh, P. S. (2022) Recent progress of Ag/TiO_2 photocatalyst for wastewater treatment: Doping, co-doping, and green materials functionalization. *Applied Materials Today*, **27**, 101500.

16. Bhardwaj, D. & Singh, R. (2021) Green biomemetic synthesis of Ag–TiO_2 nanocomposite using Origanum majorana leaf extract under sonication and their biological activities. *Bioresources and Bioprocessing*, **8(1)**.

17. Muneeb, A., Rafique, M. S., Murtaza, M. G., Arshad, T., Shahadat, I., Rafique, M. & Nazir, A. (2023) Fabrication of Ag–TiO_2 nanocomposite employing dielectric barrier discharge plasma for photodegradation of methylene blue. *Physica. B, Condensed Matter*, **665**, 414995.

18. Kader, S., Al-Mamun, M. R., Suhan, M. B. K., Shuchi, S. B. & Islam, M. S. (2022) Enhanced photodegradation of methyl orange dye under UV irradiation using MoO_3 and Ag doped TiO_2 photocatalysts. *Environmental Technology & Innovation*, **27**, 102476.

19. Chakhtouna, H., Benzeid, H., Zari, N., Qaiss, A. E. K. & Bouhfid, R. (2021) Recent progress on Ag/TiO_2 photocatalysts: photocatalytic and bactericidal behaviors. *Environmental Science and Pollution Research*,**28(33)**, 44638–44666.

20. Maulana, D. A., Ibadurrohman, M. & Slamet, N. (2021) Synthesis of Nano-Composite Ag/TiO_2 for polyethylene microplastic degradation applications. *IOP Conference Series. Materials Science and Engineering*, **1011(1)**, 012054.

21. Link, S. & El-Sayed, M. A. (2020) Shape and size dependence of radiative, non-radiative and photothermal properties of gold nanocrystals. In *International Reviews in Physical Chemistry*, **19(3),** 409–453.

22. Yu, J. M. & Jang, J. (2023) Organic Semiconductor-Based photoelectrochemical cells for efficient Solar-to-Chemical conversion. *Catalysts*, **13(5**), 814.

23. Chen, X., Cao, J., Chen, C., Chen, A. & Zheng, W. (2024) Degradation of organic dyes with solar PEC cells based on $Bi_2S_3/BiVO_4/TiO_2$ photoanode. *Inorganic Chemistry Communications/ Inorganic Chemistry Communications (Online)*, **160**, 111849.

24. Laschuk, N. O., Easton, E. B. & Zenkina, O. V. (2021) Reducing the resistance for the use of electrochemical impedance spectroscopy analysis in materials chemistry. *RSC Advances*, **11(45)**, 27925–27936.

25. Saeidi, M., Eshaghi, A. & Aghaei, A. A. (2023) Electro-optical properties of silver nanowire thin film. *Journal of Materials Science. Materials in Electronics*, **34(2)**.

26. Berdakin, M., Soldano, G. J., Bonafe, F., Liubov, V., Aradi, B., Frauenheim, T. & Sanchez, C. G. (2022) Dynamical evolution of the Schottky barrier as a determinant contribution to electron–hole pair stabilization and photocatalysis of plasmon-induced hot carriers. *Nanoscale*, **14(7)**, 2816–2825.

27. Khlyustova, A., Sirotkin, N., Kusova, T., Kraev, A., Titov, V. & Agafonov, A. (2020) Doped TiO_2: the effect of doping elements on photocatalytic activity. *Materials Advances*, **1(5)**, 1193–1201.